Journal of the Indian Chemical Society 102 (2025) 101518

Contents lists available at ScienceDirect

Journal of the Indian Chemical Society

journal homepage: www.journals.elsevier.com/journal-of-the-indian-chemical-society

Synthesis, GC-MS, spectroscopic, chemical absorption nature in various solvent, chemical reactivity, topology analyses and molecular docking evaluation of 2(4H)-Benzofuranone, 5,6,7,7a-tetrahydro-4,4,7a-trimethyl-, (R): A first principle study

L. Bhuvaneswari [a], P. Rajesh [b,**], E. Dhanalakshmi [c], P. Muzammil [d], P. Kandan [e], Abdullah N. Alodhayb [f,g], Muthumareeswaran Muthuramamoorthy [f], Mahmoud Al-Gawati [f], M. Thirunavukkarasu [h], M. Raja [i,*]

[a] Department of Physics, N.K.R. Govt. Arts College for Women, Namakkal, 637001, Tamilnadu, India
[b] Department of Condensed Matter Physics, Saveetha School of Engineering, Saveetha Institute of Medical and Technical Sciences (SIMATS), Chennai, 602105, India
[c] Department of Physics, School of Basic Science, Vels Institute of Science, Technology & Advanced Studies, Pallavaram, Chennai, 600 117, Tamilnadu, India
[d] Department of Physics, Islamiah College (Autonomous), Vaniyambadi, Thirupattur, 635752, Tamilnadu, India
[e] PG and Research Department of Mathematics, Government Arts College, Chidambaram, Annamalai University, Annamalai Nagar, 608 002, Tamilnadu, India
[f] King Abdullah Institute for Nanotechnology, King Saud University, P.O. Box 2455, Riyadh, 11451, Saudi Arabia
[g] Department of Physics and Astronomy, College of Science, King Saud University, Riyadh 11451, Saudi Arabia
[h] Department of Physics, Vel Tech Rangarajan Dr. Sagunthala R&D Institute of Science and Technology, Avadi, Chennai, 600062, India
[i] Department of Physics, Govt. Thirumagal Mill's College, Gudiyattam, 632602, Tamilnadu, India

ARTICLE INFO

Keywords:
FT-IR
Chemical reactivity
Electron-hole distribution
Topological indices
Docking studies

ABSTRACT

Benzofuranone derivatives exhibited natural studies and extensive biological applications. The Benzofurans reveal pharmaceutical properties of anti-cancer activity than standard drugs. In this current work 2(4H)-Benzofuranone, 5,6,7,7a-tetrahydro-4,4,7a -trimethyl-, (R)- (BF5TT) structure conformed from *Aegle marmelos leaves* through GC-MS spectra. The geometry properties of BF5TT investigated by B3LYP/6–311++G(d,p) process by employs DFT computational. The FT-IR spectra on BF5TT molecules compare with theoretical wavenumbers interpreted Veda 04 program. The experimental UV–Visible spectra wavelength good correlated with TD-SCF using solvation model of IEFPCM by gas phase and three solvents. Molecular parameter of HOMO-LUMO, kinetic energy shows reactivity, strength and MEP map exhibit nucleophilic and electrophilic region through colour coding on BF5TT using hybrid functional method same DFT level. NBO exhibit donor-acceptor connection $O_{10}\rightarrow C_2–O_{10}$ with high stabilization E(2) value 42.10 kcal/mol. Topological properties ELF, LOL, RDG and electron-hole distribution used to predict localization, delocalization of bond or lone pair to anti-bond and NCI within electron density obtain by Multiwfn 3.8 and the topological indices on BF5TT determine the potential to estimates the physical properties. The docking studies obtain to predict binding orientation of anti-cancer proteins surface on title bio-compound respectively.

1. Introduction

Benzofuran and its derivatives report many biological activities, nowadays the benzofuran exhibit against breast cancer cells, antiviral, antimicrobial, farnesyltransferase inhibitors, Angiogenesis inhibitors, pim-1 inhibitors, tubulin polymerization inhibitors and glycogen synthase kinase 3b inhibitors, multidrug resistance-reversing activity, inhibitors of human peptide deformylase those activities are done by natural benzofuran synthesis from various medicinal plants [1]. Benzofuran multi-functional hybrid as drugs such bio-molecules have the potential to be effective anti-AD medicines and are flexible [2]. The green synthesis benzofuran structure characterized by HRMS, FTIR,

* Corresponding author.
** Corresponding author.
E-mail addresses: drrajeshp6@gmail.com (P. Rajesh), raja.physics2014@gmail.com (M. Raja).

https://doi.org/10.1016/j.jics.2024.101518
Received 3 April 2024; Received in revised form 28 November 2024; Accepted 7 December 2024
Available online 9 December 2024

NMR against anti-fungal activity (five strains of pathogenic fungi) [3]. In the recent year, understanding the synthesis of several typical benzofuran substances and its biological roles will help students fully appreciate the significance of benzofurens in the area of medicinal research [4]. The Benzfuran derivatives act as fluorescent sensor and develop a microplate-based assay for Pd2+ [5]. Recent research on their distribution, biosynthesis, separation and biological functions is highlighted in this review [6]. With the aid of various in silico approaches, new benzofuran-appended oxadiazole molecular composites were developed as potential anti-TB medication targets [7]. The benzofuran derivative was determined by spectroscopic approaches such as FT-IR, 1HNMR, and mass spectrometry and that compound underwent additional testing for antifungal and bacterial effects [8].

Based on the above review there is no work done (FT-IR, UV–Vis spectrum have predicted theoretically and compared with the experimental spectra) by using BF5TT compound synthesis from medicinal plant of *Aegle marmelos* leaves. That crude extract were investigation gas chromatography-mass spectrometry (GC-MS) for structure conformation and the title compound has been characterized by Fourier-transform infrared (FT-IR) and ultraviolet–visible (UV–Vis) spectroscopy methods compared as well as DFT calculations. Geometry properties of bond length, bond angle, MEP surface, second order perturbation theory investigate of Fock Matrix in natural bond analysis (NBO) set and molecular parameter of highest occupied molecular orbital-lowest unoccupied molecular orbital (HOMO-LUMO), energy gap calculate using hybrid process B3LYP/6–311++G(d,p) level [9]. The solid phase FT-IR spectra on BF5TT molecules reported at area from 400 to 4000 cm^{-1} interpreted theoretical vibration wave numbers carried out Veda 04 program and the experimental UV–Vis spectra absorption wavelength 400-200 nm computed time dependant of TD-SCF under the integral equation formalism polarizable continuum model (IEFPCM). The FT-IR and UV–Vis spectrum have been predicted theoretically compared with experimental spectrum good agreement with each other. The electron localization function (ELF), localized orbital locator (LOL), reduced density gradient - non covalent interaction (RDG-NCI) and electron-hole distribution analysis through electron density on the molecules estimated by Multiwfn 3.8 and the topological indices on BF5TT determine the potential to estimates the physical properties. The docking studies interpreted highest negative binding energy of anti-cancer proteins (1DSF, 5AZ2) are well bind with title compound.

2. Experimental techniques and methods

The BF5TT molecules identified from *Aegle marmelos leaves* were gathered from Tiruvallur village, Tamil Nadu, India. Collected plant dried at normal temperature for five weak and dip with carbinol for intermittent shaking at 48 h after that using soxhlet apparatus to separate carbinol and crude, green synthesis of *Aegle marmelos leaves* were GC-MS investigation carried out (QP2010 Plus – Shimadzu) at SRM University, kattankulathur, Chengalpattu district, Tamil Nadu. The BF5TT compound was purchased from Sigma-Aldrich with 99 % purity. The FT-IR spectrum on BF5TT molecules have been recorded in the band at 4000–500 cm^{-1} using the KBr pellet technique. The spectrum was captured normal temperature with spectrum solution containing 4.0 cm^{-1}. The UV–Vis spectrum evaluation using 1 cm quartz cell with 0.5 nm slit width and PerkinElmer LAMBDA 950 UV-VIS-NIR spectrometer. The wavelength range used for recording the spectrum was 200–400 nm. The above spectral characterizations have been employed by IIT, Chennai, Tamil nadu, India.

3. Quantum chemical parameters calculation details

The accurate estimation of the bio-molecules outcome in a given reation can be obtained using computational models. The optimized structure of bond length and bond angle corresponding with X-ray diffraction results [10]. The electronic parameters of kinetic energy, chemical potential and electronegativity also predicted. Mulliken charges and molecular electrostatic potential (MEP) surface to predict reactive site of each molecular density, all the above mentioned calculations were estimated Gaussian 09W package using becke, 3-parameter, Lee-Yang-Parr (B3LYP) method 6–311++G(d,p) level [11,12]. The UV–Vis spectra of electronic transition, electronic properties of HOMO-LUMO, absorption band have been obtained by TD-SCF model. The examined UV–Vis spectrum exhibits strong biological activity because of high energy gap. The potential energy distribution (PED %) predicts the each vibrational assignment interpreted by using Veda o4 software [13]. The process of docking studies is popular tool in the development of drugs for exploring ligand-protein interactions described by 4.2.6 tool [14]. Chemical graph theory used to describes physical and chemical properties through topological indices [47].

4. Results and discussion

4.1. Identify biocomponants from Aegle marmelos leaves by GC-MS analysis

Identify the Bio constituents from carbinol crude of *Aegle marmelos* leaves by the GC-MS analysis as indicated within Table 1. The GC-MS revealed various bio-compounds conformed related by their peak area, molecular formula and retention time respectively [15,16]. In the present investigation the carbinol extract of *Aegle marmelos* leaves analysis Gas chromatography- Mass spectrometry that result revealed the different chemical component such as 3-O-methyl-D-glucose, Behenic acid, 2-(4-Isobutylphenyl)propanoic acid, BF5TT and 3-Buten-2-one, 4-(4-hydroxy-2,2,6-trimethyl-7- oxabicyclo[4.1.0] hept-1-yl)- Methyl tetradecanoate and the compound conformed based on retention time 18.26, 21.03, 23.12, 24.98 and 25.87,molecular weight 261.08, 340.61, 248.36, 180.24 and 224.30 and molecular formula $C_7H_{14}O_6$, $C_{22}H_{44}O_2$, $C_{16}H_{24}O_2$, $C_{11}H_{16}O_2$ and $C_{13}H_{20}O_3$ that GC assignment compound compared with mass spectral database in NIST library. In the multiple compounds we choose based on cancer activity compound BF5TT as shown in Fig. 1 for further investigation.

4.2. Optimized Molecular Structure

The optimized parameters has effect of polarity of molecules on BF5TT compound performed by DFT/B3LYP/6–311++G(d,p) process as specified in Fig. 2. In the current study, the title molecules have C_1 point group symmetry that calculated bond length (°) and bond angle (Å) correlated with available literature XRD results are good approximation are given in Table 2 [17,18]. The theoretical properties and the literature XRD bond length, bond angle of BF5TT compound was found the average difference is slightly deviation due to the computational method carried out in gaseous phase and the literature experimental values performed by solid phase respectively. The organic compound of title molecules contain benzofuran that connected to tetrahydro (substituents in a molecule) and trimethyl-which express as literature

Table 1
Bioactive Components Synthesis from *Aegle marmelos* leaves.

Name of the Compound	Molecular Formula	Molecular Weight (g/mol)	Retention Time (min)
3-O-methyl-D-glucose	$C_7H_{14}O_6$	261.08	18.26
Behenic acid	$C_{22}H_{44}O_2$	340.61	21.03
2-(4-Isobutylphenyl) propanoic acid	$C_{16}H_{24}O_2$	248.36	23.12
2(4H)-Benzofuranone, 5,6,7,7a-tetrahydro-4,4,7a-trimethyl-, (R)- (BF5TT)	$C_{11}H_{16}O_2$	180.24	24.98
3-Buten-2-one, 4-(4-hydroxy-2,2,6-trimethyl-7-oxabicyclo[4.1.0]hept-1-yl)-Methyl tetradecanoate	$C_{13}H_{20}O_3$	224.30	25.87

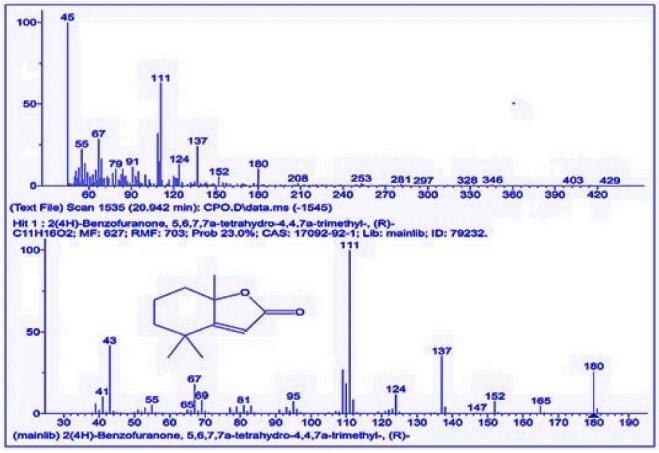

Fig. 1. GC-MS result of BF5TT.

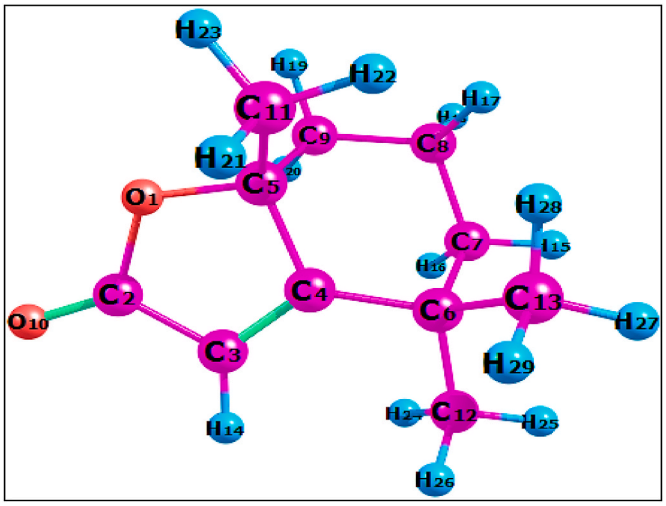

Fig. 2. Optimized molecular structure of BF5TT.

experimental bond length values are O_1–C_2→1.358, C_2–C_3→1.495, C_2–O_{10} → 1.208, C_3–C_4→1.382, C_3–H_{14} → 0.930 and C_4–C_6→ 1.489° and the literature XRD angle values are C_2–O_1–C_5→ 110.83, O_1–C_2–O_{10} → 120.95 and C_2–C_3–H_{14} → 121.2 Å are well correlated with theoretical bond lengths and bond angle respectively.

4.3. *Vibrational assingment on BF5TT molecules*

The vibrational assignment of each normal mode on $C_{11}H_{16}O_2$ compound have been interpreted B3LYP/6–311++G(d,p) level with PED % obtained by Veda 04 software [19]. That theoretical data compared with experimental prediction of harmonic vibrational assignment on title compound as given in Table 3. That $C_{11}H_{16}O_2$ molecules contain of 29 atoms which having 81 normal modes of vibrations and the quantum chemical calculation spectra with scaled values 0.963 correlated with literature survey of some functional group's corresponding values of FT-IR spectra on title molecules as illustrated in Fig. 3 respectively [20,21].

4.3.1. *C–O stretching frequency*

In C–O band on literature survey occurs area at 970-1250 cm^{-1} [22]. In the present investigation of C–O band were recorded in the boundaries at 978, 1012 cm^{-1} with high intensity in FT-IR spectra, while the computational FT-IR spectra computed with density functional theory values occur in 972, 1008 cm^{-1} with 12 % of PED. The C═O band were

Table 2
Optimized Geometrical Parameters on BF5TT compound.

Bond length (Å)	B3LYP/ 6–311++G (d, p)	XRD Values	Bond Angle (°)	B3LYP/ 6–311++G (d, p)	XRD Values
(O_1–C_2)	1.376	1.358	(C_4–C_5–C_9)	108.931	107.81
(O_1–C_5)	1.447	1.475	(C_4–C_5–C_{11})	115.571	115.86
(C_2–C_3)	1.477	1.495	(C_9–C_5–C_{11})	112.447	–
(C_2–O_{10})	1.206	1.208	(C_4–C_6–C_7)	106.408	105.30
(C_3–C_4)	1.340	1.382	(C_4–C_6–C_{12})	110.794	–
(C_3–H_{14})	1.081	0.930	(C_4–C_6–C_{13})	112.059	–
(C_4–C_5)	1.526	1.504	(C_7–C_6–C_{12})	109.027	–
(C_4–C_6)	1.515	1.489	(C_7–C_6–C_{13})	110.560	–
(C_5–C_9)	1.540	–	(C_{12}–C_6–C_{13})	107.970	–
(C_5–C_{11})	1.536	1.412	(C_6–C_7–C_8)	114.583	–
(C_6–C_7)	1.561	–	(C_6–C_7–H_{15})	108.607	–
(C_6–C_{12})	1.539	–	(C_6–C_7–H_{16})	107.948	–
(C_6–C_{13})	1.548	–	(C_8–C_7–H_{15})	110.327	
(C_7–C_8)	1.536	1.467	(C_8–C_7–H_{16})	108.444	–
(C_7–H_{15})	1.096	–	(H_{15}–C_7–H_{16})	106.608	–
(C_7–H_{16})	1.097	–	(C_7–C_8–C_9)	111.865	–
(C_8–C_9)	1.538	–	(C_7–C_8–H_{17})	110.341	–
(C_8–H_{17})	1.096	–	(C_7–C_8–H_{18})	109.189	109.5
(C_8–H_{18})	1.095	0.930	(C_9–C_8–H_{17})	110.155	
(C_9–H_{19})	1.095	0.930	(C_9–C_8–H_{18})	109.270	–
(C_9–H_{20})	1.096	–	(H_{17}–C_8–H_{18})	105.838	–
(C_{11}–H_{21})	1.093	0.960	(C_5–C_9–C_8)	110.918	–
(C_{11}–H_{22})	1.091	0.960	(C_5–C_9–H_{19})	109.872	109.5
(C_{11}–H_{23})	1.093	0.960	(C_5–C_9–H_{20})	107.733	–
(C_{12}–H_{24})	1.094	–	(C_8–C_9–H_{19})	111.275	–
(C_{12}–H_{25})	1.094	–	(C_8–C_9–H_{20})	109.677	109.5
(C_{12}–H_{26})	1.094	–	(H_{19}–C_9–H_{20})	107.230	–
(C_{13}–H_{27})	1.095	0.930	(C_5–C_{11}–H_{21})	110.715	–
(C_{13}–H_{28})	1.091	0.930	(C_5–C_{11}–H_{22})	112.321	–
(C_{13}–H_{29})	1.094	0.930	(C_5–C_{11}–H_{23})	108.375	–
Bond Angle (°)	**B3LYP/ 6–311++G (d, p)**		(H_{21}–C_{11}–H_{22})	108.704	–
(C_2–O_1–C_5)	110.280	110.83	(H_{21}–C_{11}–H_{23})	108.376	109.5
(O_1–C_2–C_3)	107.497	108.88	(H_{22}–C_{11}–H_{23})	108.241	109.5
(O_1–C_2–O_{10})	122.526	120.95	(C_6–C_{12}–H_{24})	111.416	–
(C_3–C_2–O_{10})	129.959	130.16	(C_6–C_{12}–H_{25})	110.094	–
(C_2–C_3–C_4)	109.782	109.70	(C_6–C_{12}–H_{26})	111.365	–
(C_2–C_3–H_{14})	121.525	121.2	(H_{24}–C_{12}–H_{25})	107.999	–
(C_4–C_3–H_{14})	128.609	–	(H_{24}–C_{12}–H_{26})	108.179	109.5
(C_3–C_4–C_5)	108.188	–	(H_{25}–C_{12}–H_{26})	107.644	–
(C_3–C_4–C_6)	129.440	129.49	(C_6–C_{13}–H_{27})	109.356	–
(C_5–C_4–C_6)	121.734	120.81	(C_6–C_{13}–H_{28})	113.132	–
(O_1–C_5–C_4)	104.111	102.78	(C_6–C_{13}–H_{29})	110.866	–
(O_1–C_5–C_9)	109.804	111.06	(H_{27}–C_{13}–H_{28})	107.516	–
(O_1–C_5–C_{11})	105.494	–	(H_{27}–C_{13}–H_{29})	107.924	–
			(H_{28}–C_{13}–H_{29})	107.861	–

seen at specific area 1800-1600 cm^{-1} [23]. The recent work of the C═O wavenumber was deducted at 1797 cm^{-1} in infrared spectra with strong transmittance. The computed spectra of C═O wavenumber has been identified near 1796 cm^{-1} and 89 % PED was observed by Veda 04 program that both FT-IR spectrum are well correlated with each other respectively.

4.3.2. *C═C, C–C vibration frequency*

The C═C frequency reported region 1650–1400 cm^{-1} [24]. In the current work on title compound of Benzofuranone in C═C stretching frequency present region 1612 cm^{-1} in FT-IR spectra well correlated with computational spectra of C═C band range 1608 cm^{-1} successively. In literature survey, the C–C extended harmonics have been predicted at 1380-1280 cm^{-1} [25]. Based on above research data in current invitation, the C–C oscillating frequencies observed nearby 1279 cm^{-1} in experimental spectra and corresponding computed spectra of C–C band appear region at 1279 cm^{-1} with low PED% contribution. The both spectral characterizations of wave numbers are contract and excellent agreement respectively.

Table 3
Experimental and Theoretical vibrational frequency on BF5TT molecules.

B3LYP/6–311++G(d, p)	Experimental cm^{-1}	Vibrational Assignments + (PED %)
Scaled	FT-IR	
534	–	υCC(10)+ δCCC(12)
637	–	υCC(11 + 16)+δOCO(10)+τHCCC (10)
662	665	γCCCC(11)
702	–	δOCC(36)+δCOC(10)
710	712	τHCCO(22)+ γOCOC(63)
764	769	υCC(14)+δCCC(10)
834	828	τHCCC(13)
846	–	υCC(11)+δHCC(11)+τHCCO(19)
854	856	τHCCO(48)
867	–	υOC(26)
883	892	υOC(21)
917	–	υCC(21)+τHCCC(12)
937	943	υCC(20)+ υOC(10)
960	–	υCC(13)+δHCC(10)
973	978	υOC(10)
993	–	υCC(11)+τHCCC(28)
1008	1012	υOC(13)
1022	1028	υCC(55)
1046	–	τHCCC(11)
1101	1108	δHCC(27)
1132	–	δHCC(10)+τHCCC(11)
1156	1195	δHCC(29)+τHCCC(23)
1165	–	δHCC(11)+τHCCC(14)
1174	–	τHCCC(11)
1201	1212	δHCC(11)
1230	1238	δHCC(16)
1276	1279	υCC(10)
1286	–	δCCC(12)
1314	1316	τHCCC(55)
1325	1327	δHCC(13)+τHCCC(44)
1337	–	δHCC(24)+τHCCC(36)
1360	–	δHCH(55)
1368	1372	δHCH(65)
1384	–	δHCH(77)
1434	1486	δHCH(50)
1440	1492	δHCH(51)
1442	–	δHCH(59)
1449	1501	δHCH(43)
1451	–	δHCH(36)
1458	–	δHCH(58)
1459	1463	δHCH(67)
1466	–	δHCH(55)
1472	1475	δHCH(54)
1608	1612	υCC(99)
1797	1797	υOC(89)
2919	2922	υCH_2(95)
2931	–	υCH(88)
2934	2936	υCH_2(92)
2938	–	υCH(96)
2940	2942	*υCH_3(97)*
2952	2953	υCH_3(96)
2962	2966	υCH_2(98)
2972	2976	υCH_2(86)
2985	2988	υCH(86)
2998	–	υCH(99)
3004	3006	υCH(98)
3007	3009	υCH(99)
3028	3028	υCH_3(99)
3041	3043	υCH_3(99)
3140	3140	υCH(99)

4.3.3. CH_3 oscillating frequency

The V(S) and V(AS) of CH_3 stretched wavenumbers are found at 2900–3100 cm^{-1} [26]. Normally, the V(AS) mode greater than V(S) mode carried out by research evaluation. Among the all methyl group, two asymmetric and two symmetric oscillating frequencies are identified in infrared spectrum 3043, 3028 cm^{-1} V(AS) and 2953, 2942 cm^{-1} C(S) with higher transmittance. The computationally estimated spectra showed on 3041, 3028 cm^{-1} V(AS) and 2952, 2940 cm^{-1} V(S) with overall potential energy 99 % V(AS), 97 % V(S) respectively. The bending and scissoring wavenumber of CH_3 assigned at 1350–1470 cm^{-1} [27] in research survey. The observed FT-IR spectra of CH_3 has determined at 1475 cm^{-1} (scissor) and 1463 cm-1 (bending) well correlated with calculated spectrum area at 1472 cm^{-1} and 1459 cm^{-1} with 60 % PED respectively.

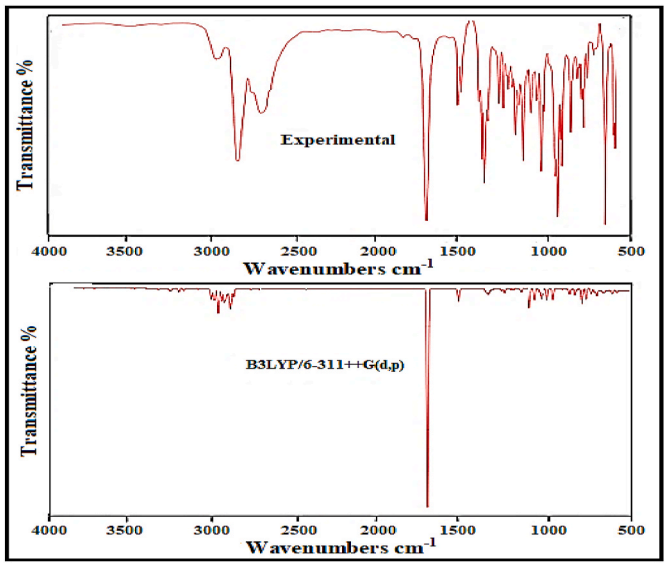

Fig. 3. FT-IR spectra compared with Theoretical Spectra on BF5TT molecules.

4.3.4. C–H vibrations

The existence of C–H oscillations stretching within area of 3100-3000 cm^{-1} was seen in the aromatic structure [28]. In this research, oscillating harmonic of C–H bands location expresses at 3009, 3009 and 2988 cm^{-1} in spectrum of FT-IR and the estimated C–H vibrational mode approximately predicted at 3007, 3004 and 2985 cm^{-1} by computational spectra. The C–H in-plane bending frequencies are occurred at area 1300-1000 cm^{-1} was in reference data [29]. In the current research, the C–H in-plane bending oscillating wavenumbers exhibit at 1238, 1212 and 1108 cm^{-1} in infra-red spectra and calculated spectra of C–H in-plane bending appear at 1230, 1201 and 1001 cm^{-1} with lower to medium PED% values are interpreted by Veda 04 software. All the above oscillating wavenumbers of C–H modes computed by B3LYP/6–311++G(d,p) level and spectral characterization of FT-IR are well correlated based on literature survey.

4.3.5. CH_2 vibrations

The oscillating modes of the CH_2 reported range at 3100 - 2900 cm^{-1} [30]. In this investigation, the V(AS) and V(S) vibration of the BF5TT compound in methylene (CH_2) group exhibits the largest concordances between estimated values and measurement results. Furthermore, the CH_2 asymmetric and symmetric oscillating harmonics are assigned at 2976, 2966 cm^{-1} V(AS) and 2936, 2922 cm^{-1} V(S) in the infra-red spectrum and correlated with the computational spectra of methylene groups asymmetric and symmetric modes are exhibit location at 2972, 2962 cm^{-1} and 2934, 2919 cm^{-1} with larger PED%. In this case CH_2 wagging wavenumbers assigned at 1327, 1316 cm^{-1} in measured spectra and compared with theoretical spectra of 1325, 1314 cm^{-1} with 55 % PED prediction.

4.4. Electronic properties

4.4.1. UV–visble spectra

The electronic transition λ (nm), oscillation strength (*f*) and band gap (eV) on the BF5TT compound carried out time density DFT/B3LYP/

6–311++G(d,p) level theory of geometry structure and contrasted with recorded UV–Vis spectra are given in Table 4 [31]. The theoretical UV–Vis spectra exhibit three energy state S1, S2 and S3 are computed by gas phase and various solvent [32]. Similarly, the experimental UV–Vis were recorded in carbinol solvent occur the range from 150 to 400 nm. The second singlet energy state (S2) has exit at 183.96 nm, oscillation strength 0.5864, band gap 6.74 eV and third singlet energy state (S3) is found 150.82 nm, oscillation strength 0.0067, band gap 8.22 eV that both states are good agreement with experimental results 185 nm and 151 nm as shown in Fig. 4 which is denoted by good pharmaceutical activity. The above beaks are corresponding to π to π* electron transition and related to the frontier orbital transition of major and minor contributions (H- > L (93 %) and H-2- > L+4 (7 %)). The first singlet energy state express 194.59 nm, oscillation strength 0.0006, band gap 6.37 eV not coincide with experimental data respectively.

4.4.2. The HOMO, LUMO and energy gap analysis

The FMOs is efficient tool for analysis electronic parameters such as HOMO-LUMO, kinetic energy, EA, IP, χ, η and ω that values are given in Table 5. The above all electronic properties describes about stability, reactivity, donating and accepting on BF5TT molecules carried out B3LYP method 6–311++G(d,p) level [33–35]. HOMO indicate electron donor which shows in red colour, while the LUMO represent electron acceptor which appear in green colour and the highest occupied molecular orbital indicate benzofurans ring in C–O bond (donor) that value is 6.9811 eV and empty molecular orbital values indicate out of benzofurans ring in C–C bond (acceptor) that value 0.9445 eV on BF5TT molecules as illustrate in Fig. 5. Those HOMO-LUMO values used to calculate energy gap 6.0366 eV which high energy gap represent low stability and high chemical reactivity that shows a well biological activity on BF5TT compound. Thereby the minus ionization potential value is −6.9811 eV and the minus electron affinity value has −0.9445 eV that electronic transition related to the Higher state, lower state of title the molecules respectively.

4.4.3. Electron hole analysis BF5TT

In the area, the DFT serves as a powerful tool verify the electronic behaviour of compound and provide a wealth of information about the distribution of electrons and holes within a compound. Heat maps are graphical representations that visually convey this complex information, making it accessible for analysis. Let's delve into the key concepts and interpretation of heat maps in the context of hole-electron analysis. The Density of surface heat map illustrates the distribution of electronic states across various energy levels within a material. A band structure provides a two-dimensional representation of energy bands in a compound. High charge density regions correspond to areas where electrons are concentrated, while low density regions indicate the presence of

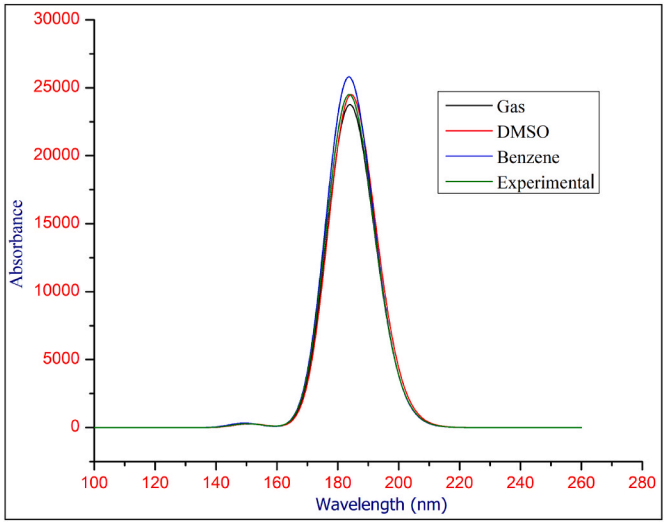

Fig. 4. Experimental and Computational UV–Vis spectra by Gas, DMSO, Benzene.

Table 5
Chemical Stability & Reactivity on BF5TT molecules.

Molecular Parameters	Gas	DMSO	Benzene
E_{HOMO} (eV)	−10.210	−10.210	−10.208
E_{LUMO} (eV)	3.033	3.034	3.083
Ionization Potential (IP)	10.210	10.210	10.208
Electron Affinity (EA)	−3.033	−3.034	−3.083
Energy gap (eV)	13.243	13.244	13.291
Electronegativity (χ)	3.588	3.588	3.562
Chemical Potential (μ)	−3.588	−3.588	−3.562
Chemical Hardness (η)	6.621	6.622	6.645
Chemical Softness (σ)	0.075	0.075	0.075
Electrophilicity Index (ω)	0.972	0.972	0.954
Nucleophilicity index (N)	1.028	1.028	1.047
Electron Donor Power ($ώ^{+}$)	3.594	3.593	3.566
Electron Acceptor Power ($ώ^{-}$)	0.005	0.005	0.004

Table 4
UV–Vis Analysis of Gas phase and different Solvent Effect on BF5TT.

Solvents	States	B3LYP/6–311++G (d,p)				Major Contributions Energy (%)	Minor Contributions Energy (%)
		Absorption band λ max (nm)	Energy cm^{-1}	Oscillation Strength (f)	Band gap (eV)		
Gas	S1	194.59	51389.16	0.0006	6.37	H-2- > L (52 %)	H-4- > L (7 %), H-2- > L+3 (3 %)
	S	183.96	54358.91	0.5864	6.74	H- > L (93 %)	H-2- > L+4 (7 %), H-1- > L (5 %)
	S3	150.82	66305.68	0.0067	8.22	H-2- > L (11 %), H-1- > L (45 %)	H-10- > L (6 %), H-7- > L (4 %)
DMSO	S1	194.73	51352.86	0.0006	6.36	H-2- > L (52 %)	H-4- > L (7 %), H-2- > L+3 (3 %)
	S2	184.39	54233.09	0.6048	6.72	H- > L (93 %)	H-2- > L+4 (7 %), H-1- > L (6 %)
	S3	150.79	66316.97	0.0069	8.22	H-2- > L (11 %), H-1- > L (45 %)	H-10- > L (6 %), H-7- > L (4 %)
Benzene	S1	199.94	50015.59	0.0003	6.20	H-2- > L (28 %), H-1- > L (36 %)	H-4- > L (5 %), H-2- > L+4 (5 %)
	S2	183.64	54454.89	0.6369	6.75	H- > L (93 %)	H-1- > L+4 (6 %)
	S3	149.30	66979.16	0.0080	8.30	H-3- > L (19 %), H-2- > L (30 %)	H-5- > L (4 %), H-4- > L (4 %)
Experimental	–	185	–	–	6.35	–	–
	–	151	–	–	8.15	–	–

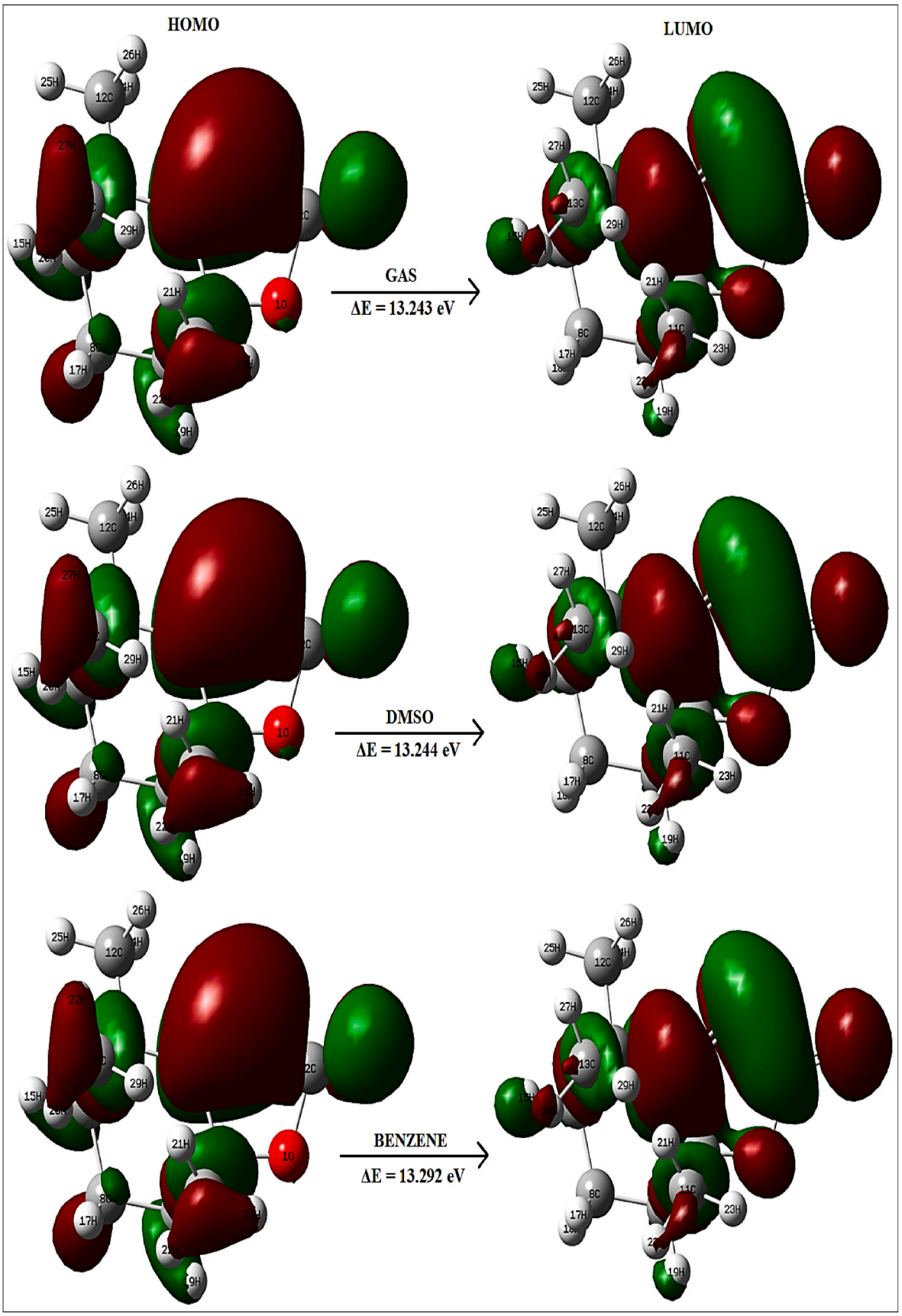

Fig. 5. Higher state & Lower state of Molecular Orbital on BF5TT Compound.

holes. Analysing the charge density provides insights into the spatial distribution and interactions of electrons and holes. Interpreting heat maps in hole-electron analysis within DFT allows researchers to gain valuable insights into the electronic properties of materials. These insights are fundamental for designing and optimizing materials for electronic devices, catalysis, and various other applications in materials science and engineering. In the present research on BF5TT revealed electron-hole distribution estimated by Multiwfn 3.8 based on B3LYP/6–311++G(d,p) approach [36]. It is a very practical way to reveal the nature of the electron excitations and electron hole analysis three excitation states with overlapping energy as indicated in Fig. 6 The first excitation state contain the C_4, C_2, O_{10}, O_1 are electron distribution along with C_1, C_3 of holes distributions. Similarly the second excitation state had C_4, C_2, O_{10}, O_1, are green with C_3, C_5, C_6 blue represent the electron and hole distribution. In the third state C_4, C_2, O_{10}, O_1 as similar with other states C_5, C_6. In S_1 state the C_4,C_2 of isosurface correlate with green, orange colour on heat map represents the electron with 0.297 A, 0.39A energy and the C_4, C_2 are blue indicate absence hole and overlapping only the electron crowd in S_1 state [37]. The C_1, C_3 of sky blue represent the holes with 0.19 A and the another two are blue with no energy on map represent absence of holes and overlapping in S_1. The electron crowd in S_1 state change the S_2 state of C_4, C_2 of isosurface correlate with green, orange, light green colour on heat map represents the electron, holes and electron hole overlapping with 0.297 A, 0.39A energy level as shown in Fig. 7. The C_3 of sky-blue, red, green represent the electrons, holes, overlapping with 0.18 A, 0.45, 0.27 energy level at state 2 excitation. In S_3 the overlapping of S1 & S2 obtained the C_4, C_2, C_3 as electron holder with 0.377 A, 0.22A,0.15A of isosurface correlate with green, skyblue, red colour on heat map. C_4 contain holes and overlapping at more energy level compared the above energy states. The C_5, C_6 of skyblue represent the holes with 0.15 A and the another two blue with no energy on map represent absence of electrons and overlapping in state 3 on title molecules successively.

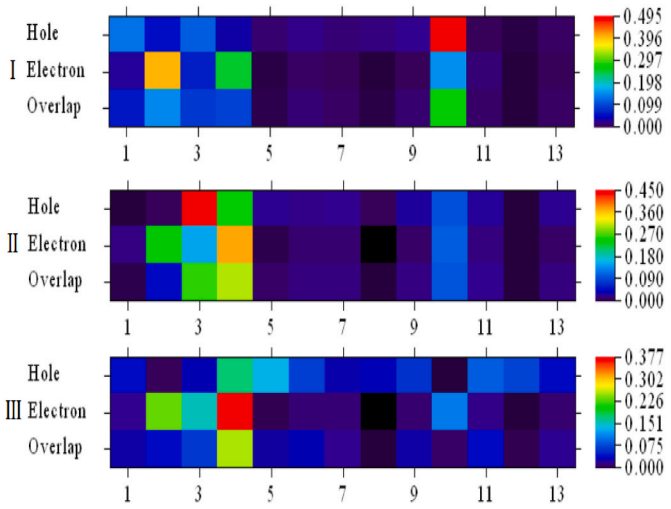

Fig. 7. The composition of Electron and Hole analysis for the three excited states of title molecule.

Table 6
NBO analysis on BF5TT.

Donor (i)	Acceptor (j)	E(2) kcal/mol	E(j)-E(i) a.u.	F(i, j) a.u.
σ O_1 - C_5	σ* C_2 - O_{10}	3.71	1.45	0.065
σ C_2 - C_3	σ* C_4 - C_6	7.92	1.10	0.084
π C_2 - O_{10}	π* C_3 - C_4	4.25	0.42	0.038
σ C_3 - C_4	σ* C_4 - C_6	5.35	1.19	0.072
π C_3 - C_4	π* C_2 - O_{10}	21.93	0.30	0.075
σ C_{11} - H_{21}	σ* C_{13} - H_{29}	10.60	0.98	0.091
σ C_{13} - H_{29}	σ* C_{11} - H_{21}	11.53	0.98	0.095
LP (2) O_1	π* C_2 - O_{10}	33.17	0.32	0.094
LP (2) O_{10}	σ* O_1 - C_2	42.10	0.52	0.134
LP (2) O_{10}	σ* C_2 - C_3	17.66	0.68	0.101
π* C_2 - O_{10}	π* C_3 - C_4	31.42	0.03	0.066

4.5. NBO analysis

The NBO used to investigate the inter-intra molecular interaction between electron-donors and electron-acceptor and hyper conjugative interaction energies was calculated from the SOPT carefully analysis by the Fock matrix as given in Table 6 [38]. The donor (i), acceptor (j) and the high stabilization energy E(2), highest electron density corresponding with delocalization i/j calculated at B3LYP/6–311++G(d,p) level using Gaussian 09 W software. In this research investigation of BF5TT compound exhibit different interactions σ→ σ*, π→ π* and LP→ π*, LP→ σ* are computed from the NBO result [39]. Among the all interactions only the two high electron density associated with LP (2) O_{10}→ σ* O_1–C_2 and LP (2) O_1→ π* C_2–O_{10} have lone pair (donor) which is oxygen atoms O_1, O_{10} to anti-bonding (acceptor) which is O_1–C_2 and C_2–O_{10} as their high stabilization energy E(2) values 42.10 and 33.17 kcal/mol respectively.

4.6. Mulliken atomic charges and MEP surface

The MEP area used to describe molecular behaviour and chemical reactivity through charge distribution of electron density in BF5TT molecules using gas phase and solvent phase carried out hybrid method

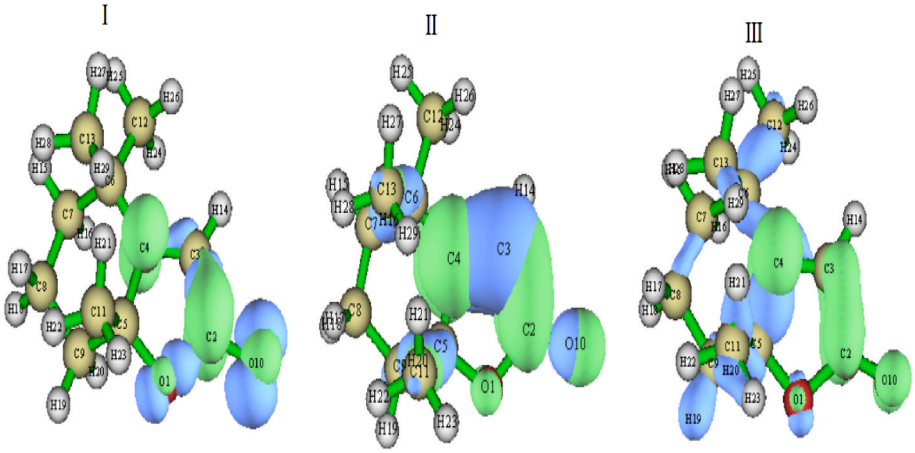

Fig. 6. Electron-Hole analysis for the three excited states of title molecule.

DFT/B3LYP/6–311++G(d,p) level [40,41]. In the title molecules has more red region represent negative area correlated with an electrophilic site and the bluest region indicate positive area associated with nucleophilic site [42]. The electrostatic potency surface of gas phase and polar, non-polar solvents colour ranges from −8.109 to +8.109 e¯2 (gas), −8.092 to +8.092 e¯2 (DMSO) and −7.418 to + 70418 e¯2 (benzene) as shows in Fig. 8. The highest negative electro potential occurs in the area carbonyl group O_{10}→-0.463 and O_1→-0.541 a.u that are given in Table 7 connected to the carbon atom which is electrophilic site (donor) negativily charged and the more positive electro potential present in the region around hydrogen atoms for example H29→+0.117 and H24→+0.136 a.u in the Benzofuranone ring which is nucleophilic site (acceptor) positively charged on BF5TT compound respectively. The gas phase and DMSO exhibit reactive ranges are well correlated which associated high electron density and greater pharmacological effect greater than benzene solvent of BF5TT molecules respectively.

4.7. Topological properties on BF5TT

4.7.1. ELF and LOL investigation

The LOL describes the bonding and non-bonding among localized kinetic energy which expressed the electron density of molecules. The electron localized function report bonding and non-bonding among delocalized kinetic energy which indicate neighbourhood electron located point or same spin. The localized electron means capture between the atoms and restricted to certain area amongst two atoms on the other hand, the delocalized electrons are scattering across several atoms

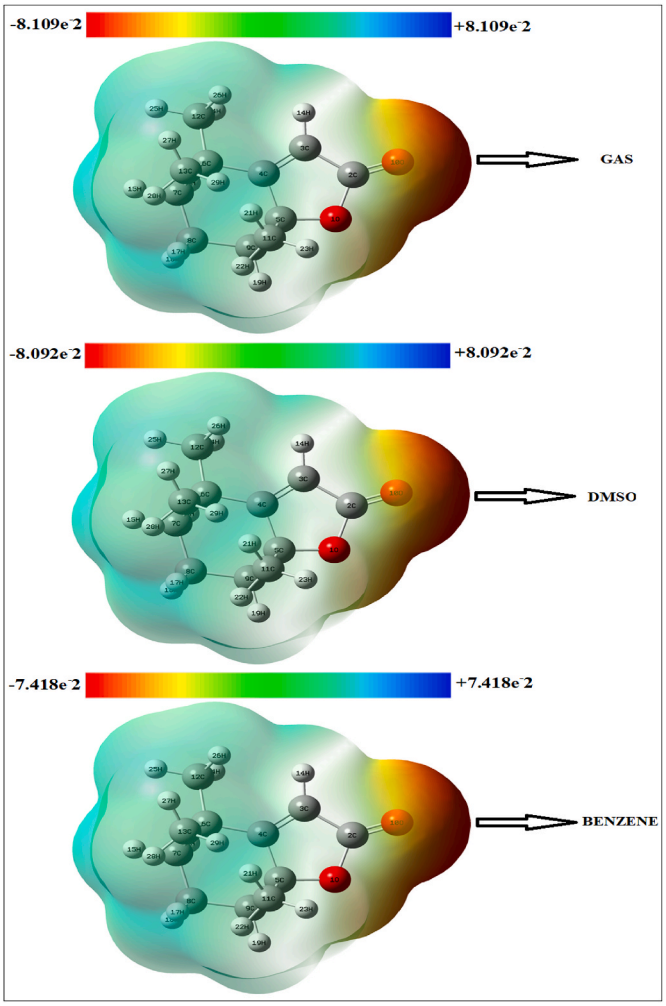

Fig. 8. MEP surface of BF5TT molecules.

Table 7
Mulliken charges on BF5TT.

S. No	Atoms	Charges (a.u)	S. No	Atoms	Charges (a.u)
1	O	−0.541	16	H	0.096
2	C	0.600	17	H	0.096
3	C	−0.208	18	H	0.106
4	C	0.106	19	H	0.107
5	C	0.294	20	H	0.104
6	C	0.037	21	H	0.110
7	C	−0.173	22	H	0.112
8	C	−0.204	23	H	0.136
9	C	−0.193	24	H	0.106
10	O	−0.463	25	H	0.099
11	C	−0.338	26	H	0.104
12	C	−0.314	27	H	0.109
13	C	−0.325	28	H	0.108
14	C	0.108	29	H	0.117
15	H	0.096			

and specifically located both below and above the atoms of the compound. The present study, the LOL and ELF's colour filled with contour chart on title compound interpreted by highly effect Multiwfn 3.8 software [43]. The localized electrons are demonstrated in the red colour area and the region between 0.00 and 0.80 Bohr as displayed in Fig. 9. While the delocalized electrons are shows across the blue colour region and the range from 0.00 to 0.10 Bohr are illustrated in Fig. 10 [44]. The ELF and LOL used to predict covalent bonding and non-bonding of strongest localized electrons are H_{14}, H_{21} and H_{22} by dark blue circle. Similarly, ELF and LOL expressed the bonding and non-bonding of strongest delocalized electrons zone predicted in C2, C4, C5 and C6 by dark red region on BF5TT molecules respectively.

4.7.2. RDG investigation on BF5TT

The RDG plot used to describes the non-covalent interactions according to electron density of molecules. Furthermore, the topological properties of RDG's investigation occur in three interactions namely the Van der Waal bonds and hydrogen bonds interaction are weak electrostatic force and the steric effects are NCI which dictate the shape and reactivity on the molecules as shown in Fig. 11 [45]. The RDG analysis stated by using the formula given below

$$RDG = \frac{1}{2(3\pi x^2)1/3} + \frac{\Delta\rho(r)}{\rho(r)4/3}$$

where ρ (r) denoted by different electron density amongst three interactions and the BF5TT molecular have been predict three interaction zones from the RDG's plots λ2 (ρ >o), λ2 (ρ <o) and λ2 (ρ = o). If λ2 (ρ >o) consider as steric effect, λ2 (ρ <o) represent hydrogen bonds and λ2 (ρ = o) indicates Van der Waal bonds interactions [46]. The red area shows highest electron density from 0.020 to 0.050 a.u, the blue region expresses low electron density from −0.020 to −0.050 a.u and the green zone expressed neutral electron density from −0.10 to +0.10 a.u of the title molecules respectively.

4.8. Chemical graph theory of BF5TT

The chemical graph theory used to describes pharmaceutical chemical compounds as chemical graph. The graph theory connects molecular structure as edges indicate atom and vertices represent bonds among the two atoms which applied by mathematical to physical and biological properties [47]. The topological indices have the potential to estimates the physical and chemical application and biological activities of chemical substances. The molecular graph's details and characteristics are frequently associated through the use of topological formula and distance-based graphical indicators [48]. The QSPR and QSAR models can be developed and modified through some variable in the topological index calculation based on distance-degree, molecular connectivity, graph distance and polynomials of molecular descriptors [49,50]. In the

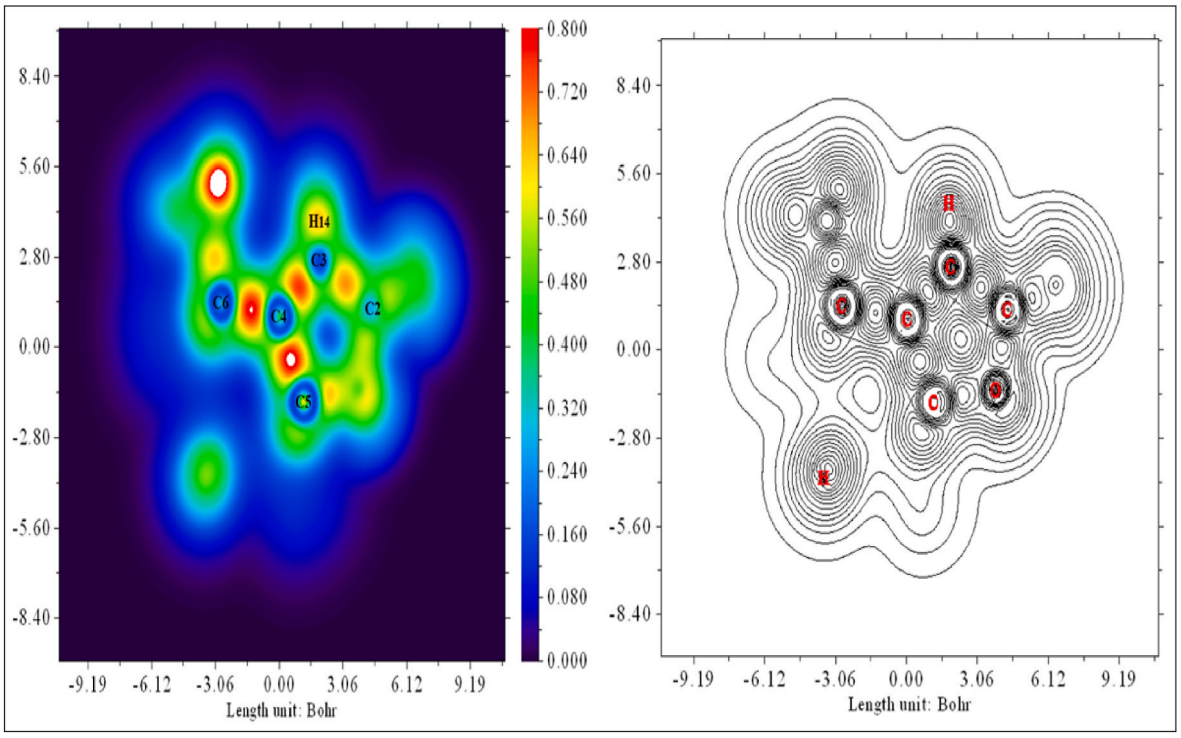

Fig. 9. Contour-line with colour-filed chart by LOL on BF5TT.

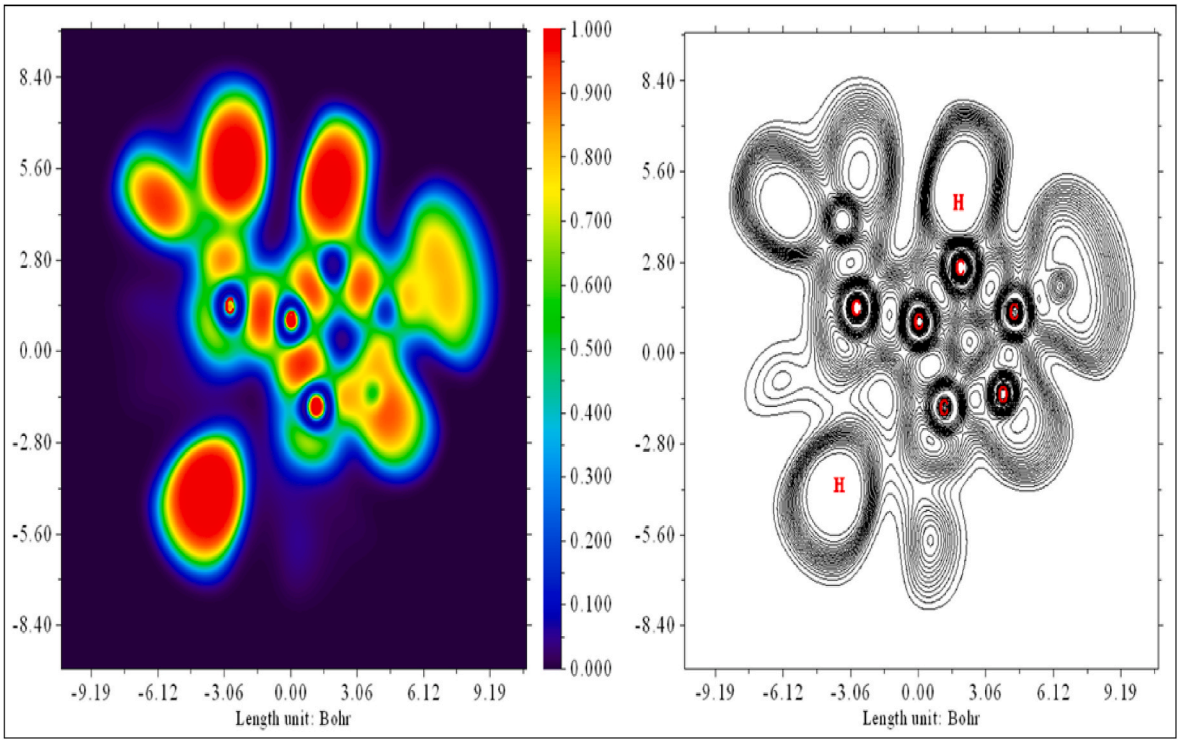

Fig. 10. Contour-line with colour-filed chart by ELF on BF5TT.

current research going to demonstrate the accurate assessment of topological descriptors for chemical molecular graph G = (V, E) based on the degree of edges E(G) and vertices V(G) which represent by d(s) and d (t) on BF5TT cancer-activity compound. Furthermore, the derivatives of benzofurans demonstrate biological and pharmacological activities, including anti-cancer properties [51] exhibit the various degree-based topological indices interpreted by

Definition 5.1. The Randic index or connectivity intex by 1975 [52] is given below

$$\chi(G) = \sum_{st \in E(G)} \frac{1}{\sqrt{d_s d_t}}$$

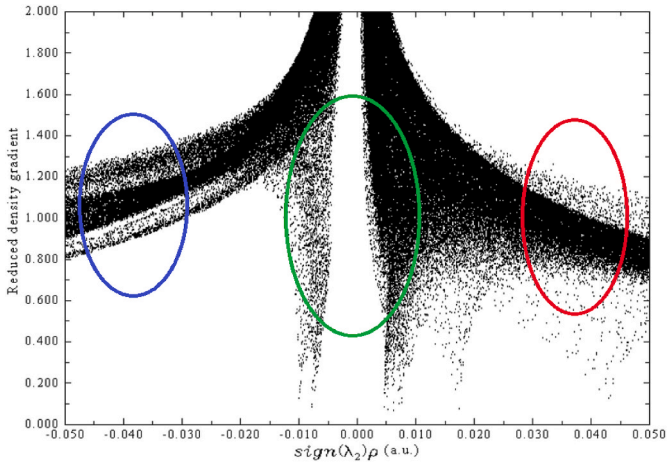

Fig. 11. RDG non-covalent interaction surface map on BF5TT.

Definition 5.2. The Zagreb indices of first and second are establish by Trinajestic and Gutman [52],

$$M_1(G) = \sum_{st\in E(G)} (d_s + d_t)$$

and

$$M_2(G) = \sum_{st\in E(G)} d_s d_t$$

Definition 5.3. the inverce symmetric division deg (ISDD) index [52] follows as

$$ISSD(\mathrm{G}) = \sum_{\mathrm{st}\in \mathrm{E(G)}} \left[\frac{P}{Q} + \frac{Q}{P}\right]$$

Definition 5.4. In Ref. [53], ABC index G is defined by

$$\mathrm{ABC(G)} = \sum_{\mathrm{st}\in \mathrm{E(G)}} \sqrt{\left(\frac{d_s + d_t - 2}{\mathrm{d_s d_t}}\right)}$$

Definition 5.5. geometric-arithmetic (GA) index interpret by

$$\mathrm{GA(G)} = \sum_{\mathrm{st}\in \mathrm{E(G)}} \frac{2\sqrt{d_s d_t}}{d_s + d_t}$$

Definition 5.6. the S(G) index [53], which is characterized as

$$\mathrm{S(G)} = \sum_{\mathrm{st}\in \mathrm{E(G)}} \frac{1}{\sqrt{d_s + d_t}}$$

Definition 5.7. H(G) index in Ref. [53], commuted by Fajtlowicz follows as

$$H(\mathrm{G}) = \sum_{\mathrm{st}\in \mathrm{E(G)}} \frac{2}{d_s + d_t}$$

Definition 5.8. In Ref. [53], describes the hyper Zagreb index defined by

$$HM(\mathrm{G}) = \sum_{\mathrm{st}\in \mathrm{E(G)}} (d_s + d_t)^2$$

Definition 5.9. The F(G) index [53] described as

$$F(\mathrm{G}) = \sum_{\mathrm{st}\in \mathrm{E(G)}} \left[(d_s)^2 + (d_t)^2\right]$$

Definition 5.10. The 3rd Zagreb index [53] has given below

$$ZG_3(\mathrm{G}) = \sum_{\mathrm{st}\in \mathrm{E(G)}} |d_s - d_t|$$

where, M = min $[d_G(s), d_G(t)]$ and N = max $[d_G(s), d_G(t)]$

The BF5TT molecules used to negleted the hydrogen atoms from optimized structure which able to identify the degree-based toplological indeces indicates earlier to derive the edge partision techniques.

Theorem 5.1. *The various degree-based topological indices of G are given below if G is the molecular graph of BF5TT compound*

$M_1(BF5TT) = 16$, $M_2(BF5TT) = 14$, $ABC(BF5TT) = 3.038$, $\chi(BF5TT) = 2.268$, $GA(BF5TT) = 4.791$, $S(BF5TT) = 2.024$, $H(BF5TT) = 2.066$, $HM(BF5TT) = 66$, $F(BF5TT) = 38$, $ZG_3(BF5TT) = 06$ and $SSD(BF5TT) = 11.332$.

Proof.

Let G be the graph of BF5TT and *E (i,j) represent the class of edges of G connecting vertices with degree i to degree j. From the optimized structure detect that* $|E_{1,3}| = 1$, $|E_{3,2}| = 3$, $|E_{2,4}| = 3$, $|E_{4,1}| = 3$, $|E_{2,2}| = 2$, $|E_{4,3}| = 2$,

(iii) *The result of using applying* 5.1., *is as follows*:

$$\chi(BF5TT) = \tfrac{1}{\sqrt{1.3}} + 3\tfrac{1}{\sqrt{3.2}} + 3\tfrac{1}{\sqrt{2.4}} + 3\tfrac{1}{\sqrt{4.1}} + 2\tfrac{1}{\sqrt{2.2}} + 2\tfrac{1}{\sqrt{4.3}} = 5.932.$$

(i) *The result that follows is the outcome of applying Principle* 5.2.

$M_1(BF5TT) = (1+3)+3(3+2)+3(2+4)+3(4+1)+2(2+2)+2(4+3) = 74$.

and

$M_2(BF5TT) = 3+3(6)+3(8)+3(4)+2(4)+2(12) = 89$.

(*x*) *By using* Definition 5.3, *we get the following*:

$$ISSD(\mathrm{BF5TT}) = 2\left[\tfrac{1}{3}+\tfrac{3}{1}\right] + \left[\tfrac{2}{3}+\tfrac{3}{2}\right] + \left[\tfrac{1}{2}+\tfrac{2}{1}\right] = 11.332.$$

(ii) *The following of using condition* 5.4, *is as follows*:

$$ABC(BF5TT) = \sqrt{\left(\tfrac{1+3-2}{1.3}\right)} + 3\sqrt{\left(\tfrac{3+2-2}{3.2}\right)} + 3\sqrt{\left(\tfrac{2+4-2}{2.4}\right)} + 3\sqrt{\left(\tfrac{4+1-2}{1.4}\right)} + 2\sqrt{\left(\tfrac{2+2-2}{2.2}\right)} + 2\sqrt{\left(\tfrac{4+3-2}{4.3}\right)} = 10.346.$$

(iv) *By using the* definition 5.5, *that following results are obtained*:

$$GA(BF5TT) = \left(\tfrac{2\sqrt{1.3}}{1+3}\right) + 3\left(\tfrac{2\sqrt{3.2}}{3+2}\right) + 3\left(\tfrac{2\sqrt{2.4}}{2+4}\right) + 3\left(\tfrac{2\sqrt{1.4}}{1+4}\right) + 2\left(\tfrac{2\sqrt{2.2}}{2+2}\right) + 2\left(\tfrac{2\sqrt{4.3}}{4+3}\right) = 13.007.$$

(v) *By using the theorem* 5.6, *the following results are obtained*:

$$S(BF5TT) = 2\frac{1}{\sqrt{1+3}} + \frac{1}{\sqrt{3+2}} + \frac{1}{\sqrt{2+1}} = 2.024.$$

(vi) *By using Principle* 5.7, *we get the result obtained*:

$$H(BF5TT) = 2\left(\frac{2}{1+3}\right) + \left(\frac{2}{3+2}\right) + \left(\frac{2}{2+1}\right) = 2.066.$$

(vii) *By using theorem* 5.8, *we get the following*:

$$HM(BF5TT) = 2(1+3)^2 + (3+2)^2 + (2+1)^2 = 66.$$

(viii) *By using principle* 5.9, *we get the following*:

$$F(BF5TT) = 2\left[1^2+3^2\right] + \left[3^2+2^2\right] + \left[2^2+1^2\right] = 38.$$

(ix) *By using* Definition 5.10, *we get the following*:

$$ZG_3(BF5TT) = 2|1-3| + |3-2| + |2-1| = 06$$

Using these topological indices, we can forecast different physical features of medications and examine the computational values. The above mathematical results may prove useful to classifying the drug design based on chemical properties when assuming in the future of medicine, mathematical chemistry.

4.9. Molecular docking investigation on BF5TT

The molecular docking is among the most effective method to examine how receptor complexes behave binding orientation of tiny molecule. In this study, we used two receptors PDB ID: 5AZ2 and PDB ID: 1DSF belongs to anticancer-activity (human epiregulin and the disulfide-stabilized Fv fragment) under the classification of immunoglobulin and immune system. The 1DSF protein structure consist the lawis-related carbohydrate epitope on human cancer cells have been detected by an engineered Fv version of the B1 monoclonal antibody [54]. Similarly, the 5AZ2 target tyrosine kinase known as the epidermal growth factor receptor (EGFR) contributes in a variety of biological processes, such as cell migration and proliferation accumulated throughout human colon and breast malignancies, it is likely involved in the development of tumours [55]. The both protein are chosen as a target ligand for docking technique and the structures downloaded as PDB format from research collaborator for structure bioinformatics (RCSB) in protein data bank and the ligand downloaded as PDB format from DFT/B3LYP/6–311++G(d,p) Gaussian 09 W receptively [56,57]. Aim of the current investigation small molecules bind with protein of interaction among ligand-receptor with high affinity to identify drug potential in 2D and 3D structure of BF5TT molecules interpreted by using AutoDock 4.2 software and was examined with mgltools 1.5.6, Notepad++ 6.7.9.2, python-2.7.2 set up to visualized ligand-receptor structure on target proteins. The two receptors 5AZ2 and 1DSF exhibit potency of inhibition constant of BF5TT compound has been carried out using docking studies [58,59]. The hydrogen bonding indicates distance between ligand-protein through yellow dotted line to find amino acid of the molecules as shows in Figs. 12 and 13. The docking studies revealed binding impact, inter molecular energy and RMSD values are very good results as shown in Table 8. The molecular docking studies of synthesised BF5TT component reported well binding affinity and excellent potency inhibition against 5AZ2 and 1DSF receptors to cure the disease of anti-cancer activity.

5. Conclusion

The BF5TT structure conformed by result of the GC-MS analysis from carbinol extract of *Aegle marmelos* leaves. The complete experimental and computational spectrum evaluation Benzofuranone derivatives of the BF5TT molecules has been completed using DFT, FT-IR, and UV–Vis through B3LYP/6–311++G(d,p) set. The reactivity area of nucleophilic and electrophilic site on BF5TT molecules were performed by MEP surface and the hyperconjugative interaction LP (2) $O_{10} \rightarrow \sigma^* O_1 - C_2$ and high stabilization energy E(2) value 42.10 kcal/mol were conformed through NBO analysis. Moreover, the chemical reactivity and stability of title molecules have been calculated by the help of energy gap. The FT-

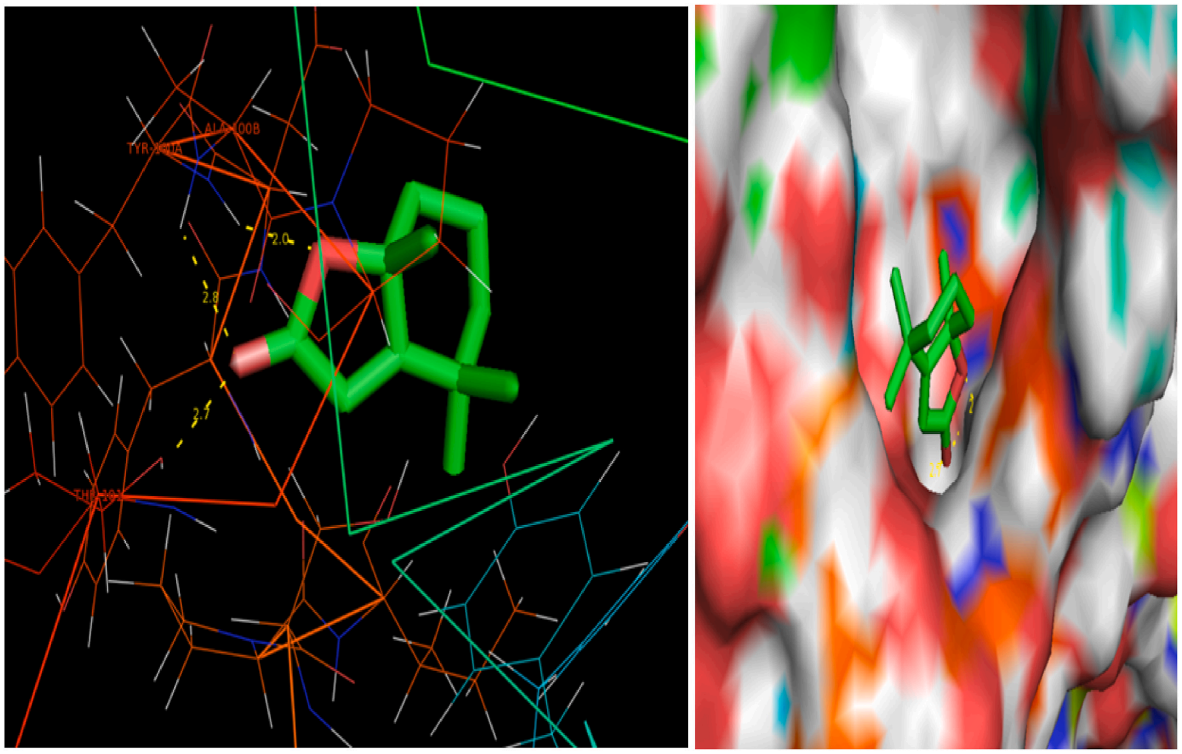

Fig. 12. Ligand-Docking Amino acid are seen in the active site on 1DSF.

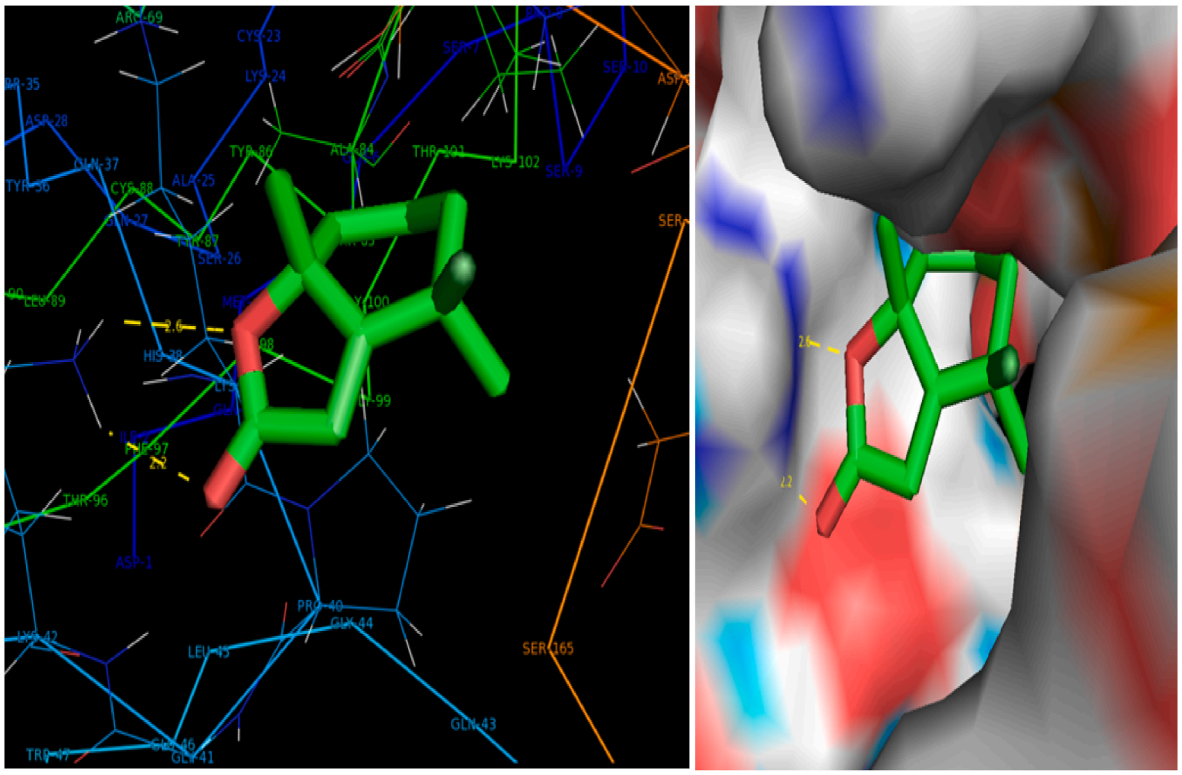

Fig. 13. Ligand-Docking Amino acid are seen in the active site on 5AZ2.

Table 8
The Binding Impact on receptors 4CG9, 4CGA with RMSD value on ONA.

Protein (PDB ID)	Bonded residues	Bond distance (Å)	Estimated Inhibition Constant (μm)	Binding impact (kcal/mol)	Inter molecular Energy (kcal/mol)	Reference RMSD (Å)
5AZ2	LYS 42 (O … HZ2)	2.2	63.03	−5.73	−6.12	47.77
	LYS 42 (O … HZ3)	2.6				
1DSF	TYR 100A (O···HN)	2.0	283.93	−4.84	−5.16	12.04
	ALA 100B (O···HN)	2.8				
	THR 101 (O···HN)	2.7				

IR spectra, intensity observed correlated with the vibrational assignment theoritically calculated with potential energy ditrubution (PED) and the UV–Visible spectrum cbserved 183.96, 150.82 nm measured by TD-SCF method well correlated with experimental UV–Visible spectra 185, 151 nm. LOL, ELF, RDG and Electron-Hole distribution through electron density was performed. The docking investigated each protein displays the smallest binding strenghths (−5.73, −4.84 kcal/mol) which demonstrate increase more efficiency for anti-cancer activity. The methematical result of BF5TT interpreted topological indices classifying the drug design based on chemical properties and forecast different physical quantities in features for medications and examine the computational values.

CRediT authorship contribution statement

L. Bhuvaneswari: Writing – review & editing, Validation, Supervision, Methodology, Investigation. **P. Rajesh:** Visualization, Supervision, Project administration, Data curation. **E. Dhanalakshmi:** Writing – review & editing, Writing – original draft, Validation, Methodology, Investigation. **P. Muzammil:** Visualization, Methodology, Investigation, Conceptualization. **P. Kandan:** Visualization, Formal analysis. **Abdullah N. Alodhayb:** Investigation, Methodology, Validation. **Muthumareeswaran Muthuramamoorthy:** Formal analysis, Investigation, Methodology. **Mahmoud Al-Gawati:** Data curation, Formal analysis, Investigation, Validation. **M. Thirunavukkarasu:** Conceptualization, Data curation, Validation. **M. Raja:** Writing – review & editing, Writing – original draft, Visualization, Supervision, Methodology, Investigation, Formal analysis, Conceptualization.

Conflict of interest

No conflict of interest exists
No conflict of interest exists in the article entitled

Acknowledgment

The author acknowledges Researchers Supporting Project number (RSPD2024R1101), King Saud University, Riyadh, Saudi Arabia, for funding this research work.

References

[1] Hena Khanam, Shamsuzzaman, Bioactive Benzofuran derivatives: a review, EJMECH 97 (2014) 1–22, https://doi.org/10.1016/j.ejmech.2014.11.039.
[2] Asha Hiremathad, Karam Chand, Rangappa S. Keri, Development of coumarin and benzofuran conjugated hybrids as the versatile multi - targeted compounds for the treatment of alzheimer's disease, Chem. Biol. Drug Des. 92 (2018) 1497–1503, https://doi.org/10.1111/cbdd.13316.

[3] Zhen Liang, Hang Xu, Ye Tian, Mengbi Guo, Xin Su, Chun Guo, Design, synthesis and antifungal activity of novel benzofuran-triazole hybrids, Molecules 21 (2016) 732, https://doi.org/10.3390/molecules21060732.
[4] Yu-hang Miao, Yu-heng Hu, Jie Yang, Teng Liu, Jie Sun, Xiao-jing Wang, Natural source, bioactivity and synthesis of benzofuran derivative, RSC Adv. 9 (2019) 27510–27540, https://doi.org/10.1039/C9RA04917G.
[5] Azumi Higashi, Naoya Kishikawa, Kaname Ohyama, Naotaka Kuroda, A simple and highly selective fluorescent sensor for palladium based on benzofuran-2-boronic acid, Tetrahedron Lett. 58 (2017) 2774–2778, https://doi.org/10.1016/j.tetlet.2017.06.005.
[6] Peter Proksch, Eloy Rodriguez, Chromenes and benzofurans of the asteraceae, their chemistry and biological significance, Phytochem 22 (1983), https://doi.org/10.1016/0031-9422(83)80118-6.
[7] Irfan Ali, Shah Faisal, Ameer Fawad Zahoor, Razia Noreen, Sami A. Al-Hussain, Burak Tuzun, Rakshanda Javaid, Ahmed A. Elhenawy, Magdi E.A. Zaki, Sajjad Ahmad, Magda H. Abdellattif, In silico development of novel benzofuran-1,3,4-oxadiazoles as lead inhibitors of M. tuberculosis polyketide synthase 13, Pharmaceuticals 16 (2023), https://doi.org/10.3390/ph16060829.
[8] Lambani Narayana Netravati, Kalapura Mathada Basavaraja, Kondareddy Gopinath Shilpa, Sharanappa veerapur bharathi, structural, spectroscopic, molecular docking and biological evaluation of some novel benzofuran derivatives, Orient. J. Chem. 38 (2022), https://doi.org/10.13005/ojc/380623.
[9] Preetika Dhawan, Anupama Saini, Karan Grover, Sahil Goel, Nidhi Tyagi, Pradeep Kumar, Ranjana Jha, Harsh Yadav, A methodical investigation on the growth and characterization of a third-order nonlinear optical novel co-crystal of 8-hydroxyquinolinium phthalate: X-ray, Hirshfeld surface, optical, mechanical, thermal and DFT analysis, Mater. Res. Bull. 169 (2024), https://doi.org/10.1016/j.materresbull.2023.112516.
[10] S. Renuga, S. Muthu, Molecular structure, normal coordinate analysis, harmonic vibrational frequencies, NBO, HOMO–LUMO analysis and detonation properties of (*S*)-2-(2-oxopyrrolidin-1-yl) butanamide by density functional methods, Spectrochim. Acta Mol. Biomol. Spectrosc. 118 (2014) 702–715, https://doi.org/10.1016/j.saa.2013.09.055.
[11] Vishnu A. Adole, DFT calculations on three 2,3-dihydrobenzofuran linked chalcones: structural, HOMO-LUMO and spectroscopic (UV-Vis and IR) interpretation, Vietnam J. Chem. 61 (2022), https://doi.org/10.1002/vjch.202100023.
[12] Sławomir Ostrowski, Jan Cz Dobrowolski, Jacek Kijeński, Vibrational spectra of isopropyl alcohol interacting with metal oxides A DFT study, J. Mol. Struct. 744–747 (2005) 893–900, https://doi.org/10.1016/j.molstruc.2004.12.020.
[13] V.S. Jeba Reeda, V. Bena Jothy, Vibrational spectroscopic, quantum computational (DFT), reactivity (ELF, LOL and Fukui), molecular docking studies and molecular dynamic simulation on (6-methoxy-2-oxo-2H-chromen-4-yl) methyl morpholine-4-carbodithioate, J. Mol. Liq. 371 (2023), https://doi.org/10.1016/j.molliq.2022.121147.
[14] S. Selvakumari, Krishna Murthy Potla, D. Shanthi, Ahmad Irfan, S. Muthu, Solvent effect on molecular, electronic parameters, topological analysis and Fukui function evaluation with biological studies of imidazo [1, 2-a] pyridine-8-carboxylic acid, J. Mol. Liq. 382 (2023), https://doi.org/10.1016/j.molliq.2023.121863.
[15] P. Lalitha, A. Parthiban, V. Sachithanandam, R. Purvaja, R. Ramesh, Antibacterial and antioxidant potential of GC-MS analysis of crude ethyl acetate extract from the tropical mangrove plant Avicennia officinalis L, South Afr. J. Bot. 142 (2021) 149–155, https://doi.org/10.1016/j.sajb.2021.06.023.
[16] C.A. Ukwubilea, A. Ahmeda, U.A. Katsayal, J. Ya'u, S. Mejida, GC–MS analysis of bioactive compounds from Melastomastrum capitatum (Vahl) Fern. leaf methanol extract: an anticancer plant, Sci. Afr. 3 (2019), https://doi.org/10.1016/j.sciaf.2019.e00059.
[17] J. Priscilla, D. Arul Dhas, I. Hubert Joe, A. Ronaldo Anuf, Spectroscopic investigation, DFT calculations, anti-inflammatory activity and molecular dynamic simulation study on fagaramide alkaloid, PACs 42 (2022) 4817–4842, https://doi.org/10.1080/10406638.2022.2094973.
[18] Rodolfo Moreno-Fuquen, Juan C. Castillo, Rodrigo Abonia, Javier Ellena, Juan C. Tenorio, (±)-3-(5-Amino-3-methyl-1-phenyl-1H-pyrazol-4-yl)-2-benzo-furan-1 (3H)-one, Acta Cryst. E 69 (2013) o1181–o1182, https://doi.org/10.1107/S1600536813017479.
[19] Eze A. Adindu, Obinna C. Godfrey, Eyuwa I. Agwupuye, Bassey O. Ekpong, Daniel C. Agurokpon, Sopuruchukwu E. Ogbodo, Innocent Benjamin, Hitler Louis, Structural analysis, reactivity descriptors (HOMO-LUMO, ELF, NBO), effect of polar (DMSO, EtOH, H2O) solvation, and libido-enhancing potential of resveratrol by molecular docking, Chem. Phys. Impact 7 (2023), https://doi.org/10.1016/j.chphi.2023.100296.
[20] V.S. Jeba Reeda, V. Bena Jothy, Vibrational spectroscopic, quantum computational (DFT), reactivity (ELF, LOL and Fukui), molecular docking studies and molecular dynamic simulation on (6-methoxy-2-oxo-2H-chromen-4-yl) methylmorpholine-4-carbodithioate, J. Mol. Liq. 371 (2023), https://doi.org/10.1016/j.molliq.2022.121147.
[21] E. Elamurugu Porchelvi, S. Muthu, Vibrational spectra, molecular structure, natural bond orbital, first order hyperpolarizability, thermodynamic analysis and normal coordinate analysis of Salicylaldehyde p-methylphenylthiosemicarbazone by density functional method, Spectrochim. Acta Mol. Biomol. Spectrosc. 134 (2015) 453–464, https://doi.org/10.1016/j.saa.2014.06.018.
[22] Shashi Janeoo, Amandeep Saroa Reenub, Rakesh Kumar, Harminder Kaur, Computational investigation of bioactive 2,3-diaryl quinolines using DFT method: FT- IR, NMR spectra, NBO, NLO, HOMO-LUMO transitions, and quantum-chemical properties, J. Mol. Struct. 1253 (2022), https://doi.org/10.1016/j.molstruc.2021.132285.
[23] Jilu Lukose, C. Yohannan Panicker, Prakash S. Nayak, B. Narayana, B.K. Sarojini, C. Van Alsenoy, Abdulaziz A. Al-Saadi, Synthesis, structural and vibrational investigation on 2-Phenyl-N-(pyrazin-2- yl)acetamide combining XRD diffraction, FT-IR and NMR spectroscopies with DFT calculations, Spectrochim. Acta Mol. Biomol. Spectrosc. 135 (2015) 608–661, https://doi.org/10.1016/j.saa.2014.07.004.
[24] S.K. Alghamdi, F. Abbas, R.K. Husseinc, A.G. Alhamzani, N.T. El-Shamy, Spectroscopic characterization (IR, UV-vis), and HOMO-LUMO, MEP, NLO, NBO analysis and the antifungal activity for 4-bromo-N- (2-nitrophenyl) benzamide; using DFT modeling and in silico molecular docking, J. Mol. Struct. 1271 (2023), https://doi.org/10.1016/j.molstruc.2022.134001.
[25] P. Rajesh, P. Kandan, S. Sathish, A. Manikandan, S. Gunasekaran, T. Gnanasambandan, S. Bala Abirami, Vibrational spectroscopic, UVeVis, molecular structure and NBO analysis of Rabeprazole, J. Mol. Struct. 1137 (2017) 277–291, https://doi.org/10.1016/j.molstruc.2017.01.072.
[26] P. Rajesh, S. Gunasekaran, T. Gnanasambandan, S. Seshadri, Experimental, quantum chemical and NBO/NLMO investigations of pantoprazole, Spectrochim. Acta Mol. Biomol. Spectrosc. 136 (2015) 247–255, https://doi.org/10.1016/j.saa.2014.09.029.
[27] P. Ramesh, M. Lydia Caroline, S. Muthu, B. Narayana, M. Raja, S. Aayisha, Spectroscopic and DFT studies, Structural determination, Chemical properties and Molecular docking of 1-(3-Bromo-2-thienyl)-3-[4- (dimethylamino)-phenyl]prop-2-en-1-one, J. Mol. Struct. 1200 (2020), https://doi.org/10.1016/j.molstruc.2019.127123.
[28] V. Arjunan, R. Santhanam, S. Sakiladevi, M.K. Marchewka, S. Mohan, Synthesis and characterization of an anticoagulant 4-hydroxy-1-thiocoumarin by FTIR, FT-Raman, NMR, DFT, NBO and HOMO–LUMO analysis, J. Mol. Struct. 1037 (2013) 305–316, https://doi.org/10.1016/j.molstruc.2013.01.014.
[29] P. Rajesh, S. Gunasekaran, T. Gnanasambandan, S. Seshadri, Molecular structure and vibrational analysis of Trifluoperazine by FT-IR, FT-Raman and UV–Vis spectroscopies combined with DFT calculations, Spectrochim. Acta Mol. Biomol. Spectrosc. 137 (2015) 1184–1193, https://doi.org/10.1016/j.saa.2014.08.100.
[30] P. Rajesh, S. Gunasekaran, A. Manikandan, T. Gnanasambandan, Structural, spectral analysis of ambroxol using DFT methods, J. Mol. Struct. 1144 (2017) 379–388, https://doi.org/10.1016/j.molstruc.2017.04.116.
[31] S. Selvaraj, P. Rajkumar, K. Thirunavukkarasu, S. Gunasekaran, S. Kumaresan, Vibrational (FT-IR and FT-Raman), electronic (UV-Vis) and quantum chemical investigations on pyrogallol: a study on benzenetriol dimers, Vib. Spectrosc. 95 (2018) 16–22, https://doi.org/10.1016/j.vibspec.2018.01.003.
[32] K. Venkata Prasad, P. Venkata Ramana, Vibrational spectroscopic studies, DFT, and molecular docking investigations of 4-fluoro- 3-methyl benzophenone, Vib. Spectrosc. 126 (2023), https://doi.org/10.1016/j.vibspec.2023.103532.
[33] Rabia Basri, Muhammad Khalid, Zahid Shafiq, Muhammad Suleman Tahir, Muhammad Usman Khan, Muhammad Nawaz Tahir, Muhammad Moazzam Naseer, Ataualpa Albert Carmo Braga, Exploration of chromone-based thiosemicarbazone derivatives: SCXRD/DFT, spectral (IR, UV−Vis) characterization, and quantum chemical analysis, ACS Omega 5 (2020) 30176–30188, https://doi.org/10.1021/acsomega.0c04653.
[34] Nursabah Sarikavakli, Onur Genc, Serife Gokçe Çalişkan, Fatma Erol, Molecular docking, HOMO-LUMO and quantum chemical computation analysis of anti-glyoximehydrazone derivatives containing pyrazolone moiety and their transition metal complexes, J. Indian Chem. Soc. 100 (2023), https://doi.org/10.1016/j.jics.2023.100981.
[35] M. Maria Julie, T. Prabhu, E. Elamuruguporchelvi, Fazilath Basha Asif, S. Muthu, Ahmad Irfan, Structural (monomer and dimer), wavefunctional, NCI analysis in aqueous phase, electronic and excited state properties in different solvent atmosphere of 3-{(E)-[(3,4-dichlorophenyl)imino]methyl} benzene-1,2-diol, J. Mol. Liq. 336 (2021) 116335, https://doi.org/10.1016/j.molliq.2021.116335.
[36] Isravel Antony Danish, Jeyaraj Jebasingh Kores, Thangasamy Sasitha, John Winfred Jebaraj, N.B.O. Dft, Homo-Lumo, Nci, stability, Fukui function and hole – electron analyses of tolcapone, Comput. Theor. Chem. 1202 (2021), https://doi.org/10.1016/j.comptc.2021.113296.
[37] V. Rajmohan, S. Deepa, S. Asha, S.V. Priya, Abir Sagaama, M. Raja, Synthesis, solvation effects, spectroscopic, chemical reactivity, topological analysis and biological evaluation of 4-chloro-N-(2, 6-dichlorobenzylidene) benzohydrazide, J. Mol. Liq. 390 (2023), https://doi.org/10.1016/j.molliq.2023.122955.
[38] Mustapha Ait El Had, Mouhi Eddine Hachim, Said Byadi, Lahoucine Bahsis, Abdelouahd Oukhri, Hafid Anane, Lahcen El Ammari, Mohamed Saadi, Moha Berraho, Benharref Ahmed, Moha Taourirte, A newly synthesized β-amino-α, β-unsaturated ketone derivative of β-himachalene: structural, NBO, NLO, and molecular docking studies, Biointerface Res. Appl. Chem. 13 (2023) 83, https://doi.org/10.33263/BRIAC131.083.
[39] Jai Kishan Ojha, Gaddam Ramesh, Byru Venkatram Reddy, Structure, chemical reactivity, NBO, MEP analysis and thermodynamic parameters of pentamethyl benzene using DFT study, Chem. Phys. Impact 7 (2023), https://doi.org/10.1016/j.chphi.2023.100280.
[40] P. Ramesh, S. Muthul, B. Narayana, M. Raja, S. Aayisha, Spectroscopic and DFT studies, Structural determination, Chemical properties and Molecular docking of 1-(3-Bromo-2-thienyl)-3-[4- (dimethylamino)-phenyl]prop-2-en-1-one, J. Mol. Struct. 1200 (2020), https://doi.org/10.1016/j.molstruc.2019.127123.
[41] B. Amul, S. Muthu, M. Raja, S. Sevvanthi, Spectral, DFT and molecular docking investigations on Etodolac, J. Mol. Struct. 1195 (2019) 747–761, https://doi.org/10.1016/j.molstruc.2019.06.047.
[42] Amine Ouaket, Anas Chraka, Ihssane Raissouni, Mohamed Amin El Amrani, Mohamed Berrada, Noureddine Knouzi, Synthesis, spectroscopic (13 C/1 H-NMR, FT-IR) investigations, quantum chemical modelling (FMO, MEP, NBO analysis),

and antioxidant activity of the bis-benzimidazole molecule, J. Mol. Struct. 1259 (2022), https://doi.org/10.1016/j.molstruc.2022.132729.
[43] S. Selvakumari, Krishna Murthy Potla, D. Shanthi, Ahmad Irfan, S. Muthu, Solvent effect on molecular, electronic parameters, topological analysis and Fukui function evaluation with biological studies of imidazo [1, 2-a] pyridine-8-carboxylic acid, J. Mol. Liq. 382 (2023), https://doi.org/10.1016/j.molliq.2023.121863.
[44] M. Thirunavukkarasu, P. Prabakaran, A. Saral, Naiyf S. Alharbi, Shine Kadaikunnan, Aleksandr S. Kazachenko, S. Muthu, Molecular level solvent interaction (microscopic), electronic, covalent assembly (RDG, AIM & ELF), ADMET prediction and anti-cancer activity of 1-(4-Fluorophenyl)-1-propanone): cytotoxic agent, J. Mol. Liq. 380 (2023), https://doi.org/10.1016/j.molliq.2023.121714.
[45] T. Brintha, J. Jeni James, M. Amalanathan, P.J. Jegan Babu, M. Sony Michael Mary, Experimental and theoretical investigation of structure activity relationship on L-Lysine Monohydrate for antioxidant efficacy, Chem. Phys. Impact 7 (2023), https://doi.org/10.1016/j.chphi.2023.100311.
[46] A. Saral, R. Shahidha, M. Thirunavukkarasu, S. Muthu, Molecular structure, spectral, computational, IEFPCM investigation, and topological study on the biologically potent; cardiotonic drug 2-chloroquinolin-3-amine with structural optimization, Chem. Phys. Impact 6 (2023), https://doi.org/10.1016/j.chphi.2023.100193.
[47] Kimberly Jordan Burch, Chapter 8 - chemical applications of graph theory, Math. Phys. Theor. Chem. (2019) 261–294, https://doi.org/10.1016/B978-0-12-813651-5.00008-5.
[48] Salma Kanwal, Yasmeen Farooq, Muhammad Kamran Siddiqui, Nazeran Idrees, Asima Razzaque, Fikre Bogale Petros, Study the behavior of drug structures via chemical invariants using TOPSIS and SAW, Comput. Math. Methods Med. (2023) 1–13, https://doi.org/10.1155/2023/4262299.
[49] Ovidiu Ivanciuc, Chemical Graphs, Molecular matrices and topological indices in chemoinformatics and quantitative structure-activity relationships, Curr. Comput. Aided Drug Des. 9 (2013) 153–163, https://doi.org/10.2174/1573409911309020002.
[50] Divya Arunachalam, Manimaran Angamuthu, Computation of certain topological indices for 2D nanotubes, Ricerche mat. 72 (2021) 263–282, https://doi.org/10.1007/s11587-021-00660-7.
[51] Joviana Farhat, Lara Alzyoud, Mohammad Alwahsh, Basem Al-Omari, Structure–activity relationship of benzofuran derivatives with potential anticancer activity, Cancers 14 (2022), https://doi.org/10.3390/cancers14092196.
[52] Sourav Mondal, Arindam Dey, Nilanjan De, Anita Pal, QSPR analysis of some novel neighbourhood degree-based topological descriptors, Complex intell, Systems 7 (2021) 977–996, https://doi.org/10.1007/s40747-020-00262-0.
[53] E. Dhanalakshmi, P. Rajesh, P. Kandan, M. Kesavan, G. Jayaraman, A. Selvaraj, R. Priya, Stability of bonds, kinetic stability, energy parameters, spectral characterization, GC–MS and molecular descriptors studies on coumarine, 3-[2-(1-methyl-2-imidazolylthio)-1-oxoethyl], J. Mol. Struct. 1295 (2024), https://doi.org/10.1016/j.molstruc.2023.136544.
[54] Orna Almog, Itai Benhar, George Vasmatzis, Maria Tordova, Byungkook Lee, Ira Pastan, Gary L. Gilliland, Crystal Structure of the Disulfide-Stabilized Fv Fragment of Anticancer Antibody B1: Conformational Influence of an Engineered Disulfide Bond, vol. 31, Wiley, 1998, pp. 128–138, https://doi.org/10.1002/(SICI)1097-0134.
[55] Mariko Iijima, Motonobu Anai, Tatsuhiko Kodama, Yoshikazu Shibasaki, Epiregulin-blocking antibody inhibits epiregulin-dependent EGFR signalling, Biochem. Biophys. Res. Commun. 489 (2017) 83–88, https://doi.org/10.1016/j.bbrc.2017.03.006.
[56] Eze A. Adindu, Obinna C. Godfrey, Eyuwa I. Agwupuye, Bassey O. Ekpong, Daniel C. Agurokpon, Sopuruchukwu E. Ogbodo, Innocent Benjamin, Hitler Louis, Structural analysis, reactivity descriptors (HOMO-LUMO, ELF, NBO), effect of polar (DMSO, EtOH, H2O) solvation, and libido-enhancing potential of resveratrol by molecular docking, Chem. Phys. Impact 7 (2023), https://doi.org/10.1016/j.chphi.2023.100296.
[57] K. Arulaabaranam, S. Muthu, G. Mani, A.S. Ben Geoffrey, Speculative assessment, molecular composition, PDOS, topology exploration (ELF, LOL, RDG), ligand-protein interactions, on 5-bromo-3-nitropyridine-2-carbonitrile, Heliyon 7 (2021) e07061, https://doi.org/10.1016/j.heliyon.2021.e07061.
[58] Shivaraj B. Radder, Raveendra Melavanki, Sudhir M. Hiremath, Raviraj Kusanur, Seema S. Khemalapure, S. Christopher Jeyaseelan, Synthesis, spectroscopic (FT-IR, FT-Raman, NMR & UV-Vis), reactive (ELF, LOL, Fukui), drug likeness and molecular docking insights on novel 4-[3-(3-methoxy-phenyl)-3-oxo-propenyl]-benzonitrile by experimental and computational methods, Heliyon 7 (2021) e08429, https://doi.org/10.1016/j.heliyon.2021.e08429.
[59] Sudhir M. Hiremath, Mahantesha M. Basanagouda, Seema S. Khemalapure, Ashwini Rayar, Anurag M. Rakkasagi, Varsha V. Koppa, R.T. Mahesh, S. Christopher Jeyaseelan, Structural, vibrational, fluorescence spectral features, Hirshfeld surface analysis, docking and drug likeness studies on 4-(2-bromo-4-methyl-phenoxymethyl)-6-methyl-coumarin derivative: experimental and theoretical studies, J. Photochem. Photobiol., A 431 (2022), https://doi.org/10.1016/j.jphotochem.2022.114055.